Supporting Information

For

Measurement of Exciton Transport in Conjugated Polymer Nanoparticles

Louis C. Groff, Xiaoli Wang, and Jason D. McNeill

A. Preparation and Characterization of Conjugated Polymer Nanoparticles (CPNs)

The copolymer poly[(9,9-dioctylfluorenyl-2,7-diyl)-*co*-(1,4-benzo-{2,1',3}-thiadiazole)] (PFBT, MW 10,000, polydispersity 1.7) was purchased from ADS Dyes, Inc. (Quebec, Canada). The fluorescent dye perylene red (Exalite 613) was purchased from Exciton (Dayton, OH). The fluorescent dye fluorescein was purchased from Invitrogen (Eugene, OR). The solvent tetrahydrofuran (THF, anhydrous, 99.9%) and sodium hydroxide (SigmaUltra, minimum 98%) were purchased from Sigma-Aldrich (Milwaukee, WI). All chemicals were used without further purification. Preparation of the fluorescent nanoparticles was performed using a previously described reprecipitation method.[1] The copolymer PFBT was dissolved in THF by gentle agitation and prepared at a concentration of 1000 ppm. Perylene red was dissolved in THF by gentle agitation and prepared at a concentration of 100 ppm. The solution was further diluted to 2 ppm for subsequent mixing with the polymer solution. Varying amounts of the dopant perylene red solution were mixed with the PFBT solution to produce solution mixtures with a constant concentration of 20 ppm PFBT and dopant/host fractions of 0 to 2 wt% perylene red. The mixtures were sonicated very briefly to ensure homogeneity. A 2 mL quantity of

each solution mixture was added rapidly to 8 mL of deionized water under sonication. THF was removed from the resulting nanoparticle suspensions by partial vacuum evaporation and subsequently vacuum filtered through a glass fiber prefilter to remove larger aggregates and a 0.1 μm PVDF membrane filter. The resulting nanoparticle suspensions are clear (not turbid) and stable for months with no visible signs of aggregation.

Size distributions and morphologies of undoped and perylene red doped PFBT nanoparticles were determined by atomic force microscopy (AFM). Samples were prepared by functionalizing the surface of a freshly cleaned glass coverslip with 3-aminopropyl-trimethoxysilane in anhydrous ethanol, followed by dipping in a diluted nanoparticle suspension for 40 minutes, then removing the coverslip and allowing it to dry overnight in an enclosed environment. Surface topographies were measured on an Ambios Q250 multimode AFM in tapping mode. As shown in Figure 1 in the main text, the mean diameter of the CPNs was 8 ± 2 nm. All of the perylene red doped PFBT CPN samples showed no substantial changes in mean diameter, with a similar size distribution.

UV-Vis absorption spectra were collected on a Shimadzu UV2101PC scanning spectrophotometer using 1 cm quartz cuvettes. Fluorescence spectra were collected and fluorescence quantum yield was measured using a commercial fluorimeter (Quantamaster, Photon Technology International, Inc.) using 1 cm quartz cuvettes. The UV-Vis spectra showed no variations from the undoped spectrum over the range of doping, and the absorbance of perylene red was well below the limit of detection of the instrument in the CPN suspensions. The fluorescence spectra of the CPN samples are given in Figure 2 in the main text. The decreased lifetimes of the particles as compared to

the polymer in good solvent are not likely to be due to J-aggregate formation, since little shift in the polymer absorption spectrum is observed upon nanoparticle formation (c.f. Fig. S1).

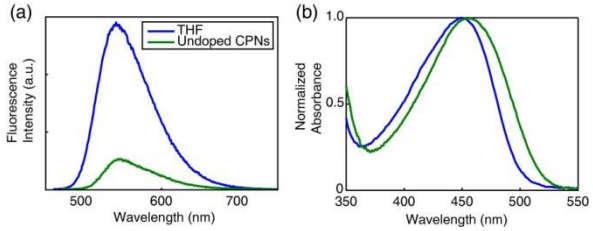

Fig. S1. (a) Fluorescence spectra and (b) normalized absorbance spectra of PFBT in THF (blue) and undoped PFBT CPNs (green).

B. Fluorescence Quantum Yield

The standard fluorescent dye fluorescein in 0.01 M sodium hydroxide was utilized to determine the fluorescence quantum yield of the PFBT CPN samples. 473 nm was selected as the excitation wavelength. The concentrations of the standard and nanoparticle suspensions were adjusted to yield an absorbance of ~0.05 at 473 nm. The absorbance, integrated fluorescence, and refractive indices of the sample and standard solutions were used in conjunction with the literature value of 0.92 for the quantum yield of fluorescein in 0.01 M sodium hydroxide to calculate the fluorescence quantum yield of the nanoparticle suspensions.[2] The results of the quantum yield measurements are given in Figure 2 in the main text.

The effect of quenching by molecular oxygen on the quantum yield of the undoped PFBT CPN samples was assessed by purging the sample with nitrogen in the dark for 45 minutes prior to measurement. The quantum yield in air was measured to be 0.097, and 0.100 in nitrogen. The differences in quantum yield for the sample in air

compared to the data in Figure 2 are not statistically significant, indicating negligible fluorescence quenching by oxygen.

C. Picosecond Time-Correlated Single Photon Counting (TCSPC) Spectroscopy

Fluorescence lifetimes were measured in air using time-correlated single photon counting (TCSPC) spectroscopy. The second harmonic (420 nm) of the output of a mode-locked Ti:Sapphire laser (Coherent Mira 900, tuned to 840 nm, ~150 fs pulsewidth, 76 MHz) was used to excite the samples. The output of a fast PIN diode (Thorlabs DET210) monitoring the pulse shape was used as the start pulse for a time-to-amplitude converter (TAC, Canberra Model 2145). Nanoparticle fluorescence was collected perpendicular to the excitation source after passing through a 460 nm long pass filter for the undoped nanoparticles. An additional 540 ±10 nm band pass filter was added for the doped samples in order to filter out the emission from perylene red. For the measurement of acceptor lifetimes, a 600 nm long pass filter was used to remove the emission from PFBT. The emission was detected by a single photon avalanche photodiode (APD, id Quantique, id100-50). The output of the APD was used as the stop pulse for the TAC. The excitation pulse was attenuated to maintain a count rate of ~6 kHz. The analog signal from the TAC was digitized using a multichannel analyzer (FastComTec, MCA-3A). Data was acquired until roughly 10^3-10^4 photons had been collected. Typical signal-to-noise ratios were above 50:1 for the samples and 100:1 for the IRF. Several TCSPC kinetics traces were obtained for each sample. Before and after each fluorescence lifetime measurement, the instrument response function (IRF) was measured using scattered laser light from a dilute suspension of polystyrene microspheres. The width of the resulting IRF was ~80 ps (FWHM). Fitting was performed using a set of custom MATLAB scripts.

Briefly, the fitting procedure is as follows. The model function consisted of either a single exponential, a bi-exponential, or a KWW decay function. Conventional gradient-based nonlinear least squares minimization methods such as Levenberg-Marquardt often fail for multi-exponential fitting, so an alternative approach was employed. A random number generator was used to generate a series of guesses for the nonlinear parameters (including shifts in t_0, since small shifts in timing can occur due to drift) over a selected range. Then, for each set of nonlinear guess parameters, the trial fit function is convolved with the instrument response function and the linear parameters (i.e., the exponential amplitudes) are determined by linear least-squares. The sum of the square of the residuals (square error) for the set of parameters is calculated and compared to the minimum square error obtained thus far. If the new value is lower, then the parameters and the square error are saved. After several thousand iterations, the set of parameters corresponding to the minimum square error is taken as the set of best-fit parameters. The soundness of the fit is tested by additional sets of iterations with both wider and narrower ranges for the guesses, and by visual inspection of the residuals. Additionally, the range of data included in the fitting analysis, as well as the degree of downsampling of the data were varied, and the effect on the resulting fit parameters was evaluated. The fitting results for several TCSPC kinetics traces for each sample were used to determine the mean and standard deviation of the parameter values. Typical standard deviations of better than 10% were obtained for the lifetime values.

The effect of quenching by molecular oxygen on the lifetime of the nanoparticle samples was also assessed by comparing the lifetime results obtained for samples exposed to air with those obtained from nitrogen-purged samples. The bi-exponential

weighted average lifetimes of the undoped PFBT CPNs were measured to be 780 ps in air and 850 ps in nitrogen. This difference is not statistically significant, and is in agreement with the quantum yield measurements indicating minimal quenching by oxygen.

In addition to the lifetimes of the host polymer PFBT, the lifetimes of the acceptor perylene red were measured. The lifetime of perylene red in THF was measured to be 5.4 ns, which is consistent with the literature value.[3] The moderate to heavily doped samples of PFBT nanoparticles were selected due to the relatively low contribution to the emission signal by PFBT as well as to assess the effect of the observed self-quenching of perylene red on its lifetime in the nanoparticles. The lifetime of perylene red doped within the nanoparticles was found to be reduced to 3.1 ns, and follows a decreasing trend as doping increases. The reduction in lifetime indicates dynamic self-quenching.

Table S1. Fluorescence lifetimes of dye-doped PFBT CPNs

Perylene Red %(w/w)	τ_{exp} (ns)*
THF	5.4
1.0%	3.1
1.5%	2.9
2.0%	2.6

*Corresponds to lifetime of the acceptor, perylene red.

D. Radiative Rate

The radiative rates of the polymer dissolved in THF and the nanoparticles suspended in water were determined as follows. For the nanoparticles, a fluorescence quantum yield (c.f. Fig. S1) of Φ = 0.14 and weighted average excited state lifetime of τ_{avg} = 800 ps was determined, while for the polymer dissolved in THF, Φ = 0.66, τ_{avg} = 3000 ps was determined. From this information and the quantum yield expression,

$$\Phi = \frac{k_r}{k_r + k_{nr}} \quad \text{(S.1)}$$

a radiative rate value for the nanoparticles of 1.8×10^8 s^{-1} was determined, while for the polymer in THF, a radiative rate of 2.2×10^8 s^{-1} was determined. As noted in the main text, this does not correspond to typical J-aggregate behavior. Rather, the radiative rate typically increases for J-aggregates as compared to the unaggregated dye.

E. Exciton Diffusion-Energy Transfer Model

We previously developed a numerical random-walk approach to modeling the combined effects of exciton diffusion and energy transfer in CPNs. Here, we have modified the previous simulation code to provide kinetics information for comparison to the time-resolved fluorescence results, and explicitly included quenching by defects. The simulation algorithm is described as follows. The simulation code was written as a set of MATLAB scripts. Dopant dyes and/or defects are distributed randomly within the nanoparticle, represented by a sphere. An initial population of excitons is also distributed randomly within the sphere. For each time step Δt, each exciton is propagated by adding to its position along each axis a Gaussian-distributed random number scaled so that $\sigma^2 = 2D\Delta t$, where D is the (1D) diffusion constant and σ^2 is the variance of the random number distribution ($\mu = 0$). A time step Δt of 1 ps was employed, and time steps of 0.2 ps, 0.5 ps, 2 ps, and 5 ps were also tested, to help ensure that the simulation results were not significantly affected by numerical rounding errors or using a step that is too large given the various rates and diffusion distances involved. At each step, the new positions are checked to ensure that the exciton remains within the sphere representing the particle, and the jump is reversed for excitons that are outside the sphere, thus ensuring that the

excitons remain within the sphere. The energy transfer rate, for each exciton to each dopant or defect, is calculated based on the exciton-acceptor distances and the conventional Förster rate expression,

$$k_{et} = \tau^{-1} \sum_{acceptors} (R_0 / R)^6 . \quad \text{(S.2)}$$

The probability of decay or transfer for a given exciton during the time step Δt is calculated by the expression

$$p(\Delta t) = 1 - e^{-k\Delta t} \quad \text{(S.3)}$$

where k is given by either $k_d = k_r + k_{nr} = \tau^{-1}$, or k_{et}, and compared to a random number to determine the exciton fate for that time step. The running total of excitons that have decayed via energy transfer is updated (for later use in determining the quenching efficiency), and the exciton population is updated (for later use in constructing a simulated kinetics trace), for each time step. The simulation continues until nearly all of the exciton population has decayed. The simulations are performed for many initial random configurations of acceptors and excitons, and the exciton population kinetics and energy transfer efficiencies are calculated from the simulation results.

The defect density per nanoparticle (expressed in dye equivalents) has been added as a model parameter in order to account for quenching by defects in CPNs. This was accomplished by explicitly accounting for the Poisson distribution of defects and dyes in the model. Exciton diffusion simulations were carried out for a particle of radius 4 nm, to match the 8 nm diameter determined by AFM (c.f. Fig. 1 in main text), with the exciton diffusion length set at 12 nm, and the time step set to 1 ps. In order to simulate a given dye and/or defect density, first the Poisson distribution of dyes or defects per nanoparticle

was calculated by $f(n;\lambda) = \frac{\lambda^n e^{-\lambda}}{n!}$, based on the average number of dyes or defects per nanoparticle, (e.g., if λ = 1.7 dyes per particle on average, the Poisson distribution is used to estimate what population fraction of particles has *n* = 0, 1, 2, or 3 dyes, and so on) and simulations were performed assuming various numbers of dyes per nanoparticle, determined from the weight ratios of perylene red dopant. Then the kinetics curves and energy transfer efficiencies were combined using Poisson statistics to produce a weighted average kinetics curve and energy transfer efficiency for the dopant density of interest. Initially, a Förster radius of 3 nm was calculated by

$$R_0^6 = \frac{9000\ln(10)\kappa^2\Phi_{THF}}{128\pi^5 N n^4}\int_0^\infty F_D(\lambda)\varepsilon_A(\lambda)\lambda^4 d\lambda, \qquad \text{(S.4)}$$

using the refractive index of PFBT at the peak emission wavelength (~1.9),[4] the spectra of perylene red $\varepsilon_A(\lambda)$ and PFBT in THF $F_D(\lambda)$, the quantum yield of PFBT in THF, and assuming a value of 2/3 for the orientation factor κ^2.[5] However, while the match to experimental lifetimes and ß values improved, the simulation results did not match experimental quenching efficiencies well. It is likely that local ordering of the polymer could result in a somewhat larger value of the orientation factor, or that other physical processes such as coherent or dispersive transport could lead to a larger quenching radius.[6,7] Thus, simulations were carried out using an increased R_0 of 4 nm. This improved the agreement with experimental quenching efficiencies. It is assumed that a combination of exciton diffusion and energy transfer in the aggregated state of the polymer are the principal causes of defect quenching in the nanoparticles. The single exponential decay kinetics and high quantum yield exhibited by the polymer in good solvent, assumed to be due to the open conformation of the polymer, as well as the

reduction in quantum yield and complex decay kinetics exhibited in the aggregated state of the polymer supports this notion. In order to quantify the defect density per nanoparticle, the fluorescence quantum yields of PFBT in THF and undoped CPNs were utilized to first estimate the defect quenching efficiency $\eta_d = 1 - (\Phi_{THF}/\Phi_{CPN})$ which yields a quenching efficiency of ~0.79. Exciton diffusion and energy transfer simulations were performed using the same model parameters as were used to model the dye-doped CPNs, varying the defect density until good agreement with the quenching efficiency, lifetime and ß of undoped CPNs was obtained, yielding a defect density of 2.3 defects per nanoparticle or 8.6×10^{18} defects per cubic centimeter of polymer.

The exciton diffusion length was then obtained by performing simulations incorporating energy transfer to perylene red dyes, adding the defect density and dye densities for each weight fraction of dye and varying the exciton diffusion length to find the best match to experimental quenching efficiencies, lifetimes, and ß. This is given in detail in the main text. Simulations neglecting quenching by defects and Poisson statistics yield a good fit to experimental quenching efficiency; however, the fits to experimental lifetimes and ß are poor (c.f. Fig S2). By accounting for quenching by defects and Poisson statistics in the model, there is a trade-off in that the fit to experimental quenching efficiency is somewhat poorer, but the match to the lifetimes and ß is greatly improved.

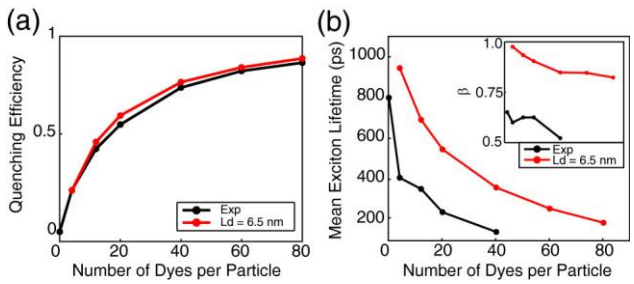

Fig S2. Exciton diffusion simulation results ignoring quenching by defects and Poisson statistics. (a) Simulated (red) and experimental (black) quenching efficiency, (b) mean exciton lifetimes, and ß (inset) as a function of dyes per nanoparticle for a particle radius of 12 nm.

Results of exciton diffusion simulations (c.f. Fig S3) indicate that an increase in *either* L_D or R_0 (or both) results in an increase in quenching efficiency. While there is no simple, exact analytical formula relating L_D and R_0 to the β parameter, we found that β increases monotonically with increasing L_D, (i.e., increasing L_D results in a decrease in the amount of heterogeneity in energy transfer rates) while β decreases as R_0 increases. By including analysis of the β parameter, as well as quenching by defects, we obtained a significantly larger value for the Förster radius than that obtained using the typical assumption of $\kappa^2 = 2/3$, suggesting that this assumption should be reexamined.[8]

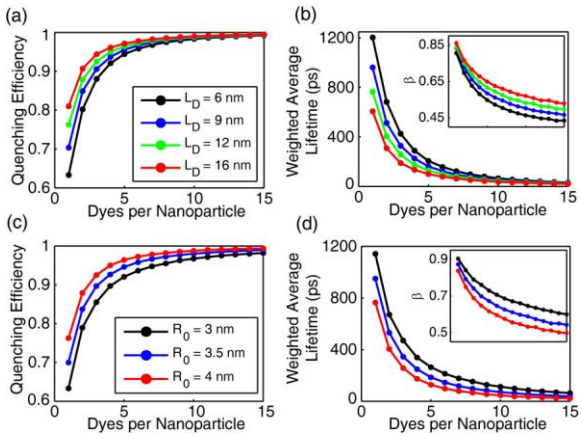

Fig. S3. Initial exciton diffusion simulations for a 4 nm particle radius. (a,b) Quenching efficiency, bi-exponential weighted average lifetime, and ß (inset) vs. dyes per nanoparticle for L_D = 6 nm (black), 9 nm (blue), 12 nm (green), and 16 nm (red). (c,d) Quenching efficiency and bi-exponential weighted average lifetime, and ß (inset) vs. dyes per nanoparticle for R_0 = 3 nm (black), 3.5 nm (blue), and 4 nm (red).

References for Supporting Information

(1) Szymanski, C., Wu, C. F., Hooper, J., Salazar, M. A., Perdomo, A., Dukes, A., McNeill, J. D. *J. Phys. Chem. B* **2005**, *109*, 8543.

(2) Weber, G., and Teale, F. W. J. *Trans. Faraday Soc.* **1957**, *53*, 646.

(3) Al-Kaysi, R. O., Ahn, T. S., Muller, A. M., and Bardeen, C. J. *Phys. Chem. Chem. Phys.* **2006**, *8*, 3453.

(4) Campoy-Quiles, M., Heliotis, G., Xia, R. D., Ariu, M., Pintani, M., Etchegoin, P., and Bradley, D. D. C. *Adv. Funct. Mater.* **2005**, *15*, 925.

(5) Lakowicz, J. R. *Principles of Fluorescence Spectroscopy*; Third ed.; Springer Science+Business Media, LLC: New York, 2006.

(6) Athanasopoulos, S., Hoffman, S. T., Bässler, H., Köhler, A., and Beljonne, D. *J. Phys. Chem. Lett.* **2013**, *4*, 1694.

(7) Scholes, G. D., and Rumbles, G. *Nat. Mater.* **2006**, *5*, 683.

(8) Wu, C. F., Zheng, Y. L., Szymanski, C., and McNeill, J. D. *J. Phys. Chem. C* **2008**, *112*, 1772.